applied sciences

MDPI

Article

A Study on Development of New Type Rubber Boot for Sleeper Floating Track System (STEDEF): Materials and Shapes

Jung-Youl Choi [1], Sun-Hee Kim [2,*], Hee Soo Park [3] and Jee-Seung Chung [1]

[1] Department of Construction Engineering, Dongyang University, Yeongju-si 36040, Republic of Korea
[2] Department of Architectural Engineering, Gachon University, Seongnam-si 13120, Republic of Korea
[3] JADOL Co., Ltd., No. 702, 221, Incheon-si 21641, Republic of Korea
* Correspondence: shkim6145@gachon.ac.kr; Tel.: +82-031-750-4718

Abstract: Urban railway sleeper floating track (STEDEF) reduces the block vibration transmitted to the subgrade structure by structurally separating the sleeper and the concrete bed, using a rubber boot and a resilient pad. Recently, the replacement of rubber boot material (SBR) after long-term wear and tear has become of utmost importance because of durability problems such as deformation, tearing, and abrasion. This study investigates rubber boots—a component of the urban railway sleeper floating track—to resolve these concerns and proposes the material and shape of a novel rubber boot. The proposed rubber boot reduces the maximum displacement and strain by more than 83% and 90%, respectively, compared with the existing rubber boots. In addition, the results of numerical analysis and indoor tests show that type 3 rubber boots can prevent displacement and stress generation in rubber boots.

Keywords: sleeper floating track; rubber boot; resilient pad; novel rubber boot

check for updates

Citation: Choi, J.-Y.; Kim, S.-H.; Park, H.S.; Chung, J.-S. A Study on Development of New Type Rubber Boot for Sleeper Floating Track System (STEDEF): Materials and Shapes. *Appl. Sci.* **2023**, *13*, 3068. https://doi.org/10.3390/app13053068

Academic Editors: Junwon Seo and Jong Wan Hu

Received: 30 January 2023
Revised: 21 February 2023
Accepted: 23 February 2023
Published: 27 February 2023

1. Introduction

Urban railway sleeper floating track (STEDEF) has a functional feature that reduces the transmission of track vibration to the subgrade structure by structurally separating the concrete bed and the sleeper. The rubber boot is an essential component of the structural separation between the concrete bed and the sleeper and is necessary to maintain the function of STEDEF. Lines 5–8 of the Seoul Metro in South Korea were laid in the 1990s and have been in use for more than 20 years. The amount of track materials being replaced or maintained is increasing owing to the aging and deterioration of the track materials, including rubber boots. The need to replace the existing rubber boots is becoming more apparent owing to durability problems, such as the deformation, tearing, and abrasion of Styrene butadiene rubber (SBR) material.

STEDEF's components continuously deteriorate and incur damage due to long-term use and repeated train load. Most prior studies on STEDEF mainly focused on deterioration and damage cause analysis, maintenance measures, and dynamic behavior targeting rails, rail pads, and resilient pads. However, studies on rubber boots have been few and far in between. In South Korea, Choi et al. [1] analyzed the need to replace resilient pads, which are track components of the STEDEF (an urban railway sleeper floating track) structure, and studied the effect of the resilient pads on the overall behavior of the track. As a result of their study, it was concluded that the timely replacement of the resilient pads is an important factor in securing the durability of the track and track materials as a whole and improving the performance life by restoring track support stiffness and reducing tracks' impact level. Lee et al. [2] performed on-site measurements for each urban railway track structure in use to calculate the track support stiffness and analyzed and compared it with the theoretical track support stiffness to experimentally suggest the range of track support stiffness for each track type and condition. Kim [3,4] analyzed the cause of damage to the track components of urban railway sleeper floating track (STEDEF) blocks in use. In the case of fastener (e-clip) damage, the lateral force of both the curved area and rail slope was dominant. Additionally, the increase in the spring stiffness of the resilient pad, due to deterioration, has the potential to cause damage to all the track components because of an increase in the reaction force of the rail support point and the amplified impact effect of the dynamic load.

A detailed view of the STEDEF and the rubber boot are shown in Figure 1.

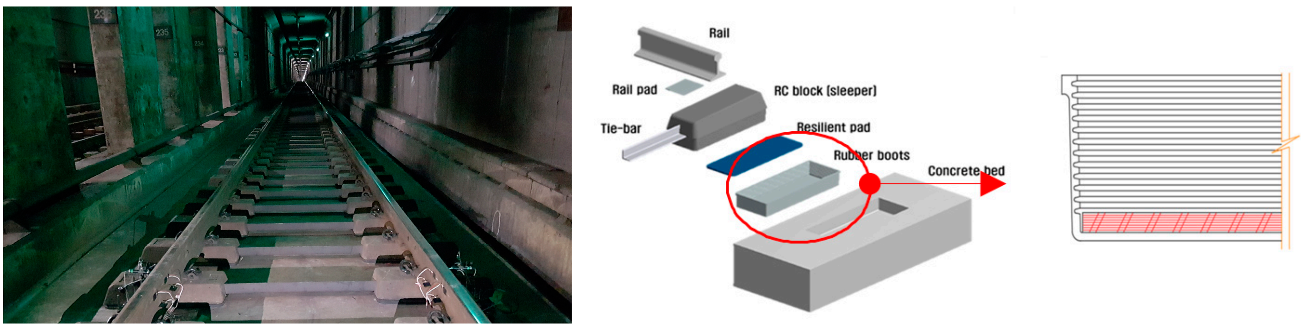

(a) (b)

Figure 1. STEDEF: (**a**) STEDEF view; (**b**) rubber boot details.

Lee [5] performed a rubber boot performance test on the track components of STEDEF blocks in use for the Busan Metro Line 2 in South Korea and analyzed the performance of the resilient pad and the rubber boot. Vu et al. [6] performed numerical analysis to precisely analyze the structural behavior of a precast slab track system and train running safety and evaluated the load-transfer efficiency. Zhou et al. [7] conducted on-site measurements, indoor tests, and numerical analyses on a track structure with an asphalt concrete waterproofing layer applied to the subgrade to confirm the effectiveness of the waterproofing layer. Cai et al. [8] conducted on-site measurements on a long elastic sleeper track (LEST), an elastic sleeper track that was recently designed and used for subways, and evaluated the vibration effects of the track structure and tunnel to confirm the vibration reduction effect of the track structure. Ferdous et al. [9,10] and Ju et al. [11] examined the performance and field applicability of sleepers by using materials such as recycled plastics and epoxy polymers for existing railway sleepers to improve their shape. Smirnov [12] analytically verified the vibration reduction effect of the resilient pad made of elastomer material on a sleeper floating track. Gupta et al. [13] used numerical analyses to evaluate the impact of vibration on structures adjacent to urban railways in use and verified the effect by applying a floating track to the section. According to previous studies [5,14], rubber boots are subject to intensive maintenance, and although they incur serious damage, as shown in Figure 2, research on rubber boots is lacking. Additionally, rubber boots for STEDEF are buried under rails and sleepers, so it is almost impossible to visually identify whether the boot is broken or damaged. Currently, when other parts are being replaced, a malfunction occurs in the rubber boot, which is then replaced. Such damage to the rubber boot cannot lead to structural separation between the concrete bed and sleepers, which directly affects the quality of the overall track and impacts train running safety by increasing the vibration, noise, and possibly damage to other track components. Therefore, in this study, a rubber boot was developed using engineering plastic (EP) to compensate for the disadvantages of the existing rubber boots made of SBR.

Figure 2. Aged rubber boots.

Actual train loads were applied to the rubber boots, and a numerical analysis was utilized to model the rubber boots made of SBR. This model was applied to analyze the cause of damage to rubber boots, and the material from which the rubber boots were made was changed to EP. In addition, the optimal rubber boots were derived by analyzing the deformation characteristics of the rubber boots according to the shape change.

The performance improvement in using the novel rubber boot was checked based on experiments and analysis.

2. Numerical Analysis

2.1. Design of Rubber Boot

Rubber boots prevent damage to the concrete ballast by structurally separating the RC sleeper and the concrete ballast and fixing the RC sleeper. The inner irregularities in rubber boxes reduce the abrasion caused by the friction between the RC sleeper and the rubber box. This is due to the mechanics of resisting the lateral movement of the sleepers. The rubber boot material is SBR (styrene butadiene rubber), which is the main component of STEDEF.

Rubber boots embedded in the concrete ballasts can be damaged by the vibration and shock generated by the train load. In addition, a significant number of rubber boots are replaced every year. In this study, a rubber boot was designed to minimize the stress concentration derived from the damage type and the analysis results that occurred in the rubber boot made of SBR material. The train load caused the sleeper to rotate left and right, and resulting in the generation of a concentrated stress on the transverse irregularities formed inside the rubber boot. Therefore, the internal unevenness in the horizontal direction of the rubber boot (Figure 3a) transformed into the vertical direction (Figure 3b), and the unevenness interval widened to increase the load resistance area.

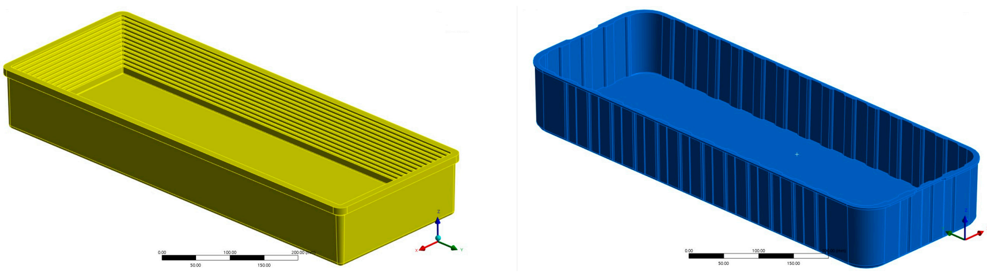

(**a**) (**b**)

Figure 3. Design of a rubber boot: (**a**) internal unevenness in the horizontal direction in the first panel; (**b**) internal unevenness in the vertical direction in the second panel.

2.2. Modeling

For the numerical analysis modeling, the rails, rail pads, RC blocks, tie bars, resilient pads, rubber boots, and concrete beds, excluding rail fasteners, were modeled as three-dimensional (3D) solid elements based on the actual design drawings, as shown in Figure 4. For the numerical analysis, ANSYS Workbench Ver.2021 R1 [15], a general-purpose structural analysis program, was used. The rubber boot was modeled as shown in Figure 4a.

The mesh of the rubber boot model contained 724,198 nodes and 387,932 elements. The STEDEF model was configured as shown in Figure 4b.

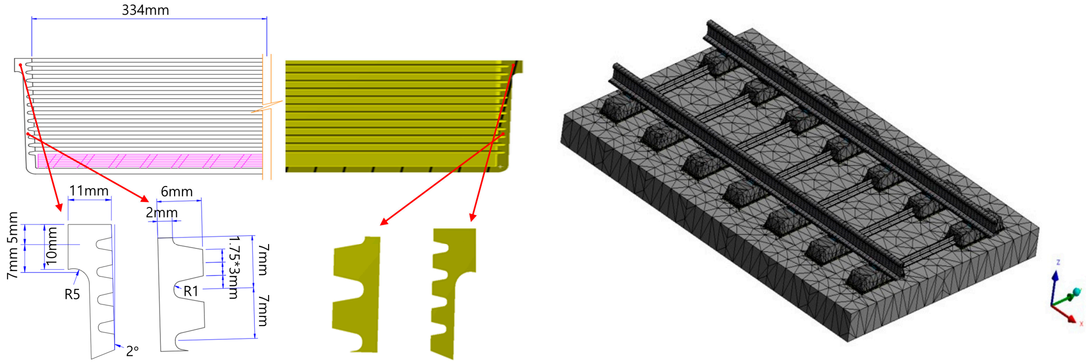

(a) (b)

Figure 4. Numerical analysis modeling: (**a**) rubber boot details; (**b**) STEDEF.

Table 1 shows the material characteristics of each track component used for the numerical analysis.

Table 1. Material characteristics of each track component.

Track Component		Material Characteristics		
		Young's Modulus (MPa)	Mass Density (kg/m^3)	Poisson's Ratio (v)
Rail		210,000	7850	0.30
Rail pad		200,000	7850	0.30
RC block		72.6	950	0.20
Tie bar		35,000	2300	0.18
Rubber boot		0.98	700	0.49
Resilient box	(SBR)	21.4	800	0.20
	(EP)	2000	1140	0.15
Concrete bed		35,000	2300	0.18

2.3. Loading and Boundary Conditions

To analyze the cause of damage to the rubber boots, the load conditions of case 1 (train load condition) and case 2 (rail longitudinal pressure condition) were used for the numerical analysis. Additionally, the boundary conditions of the two conditions were applied as fixed support and are shown in Figure 5 and Table 2.

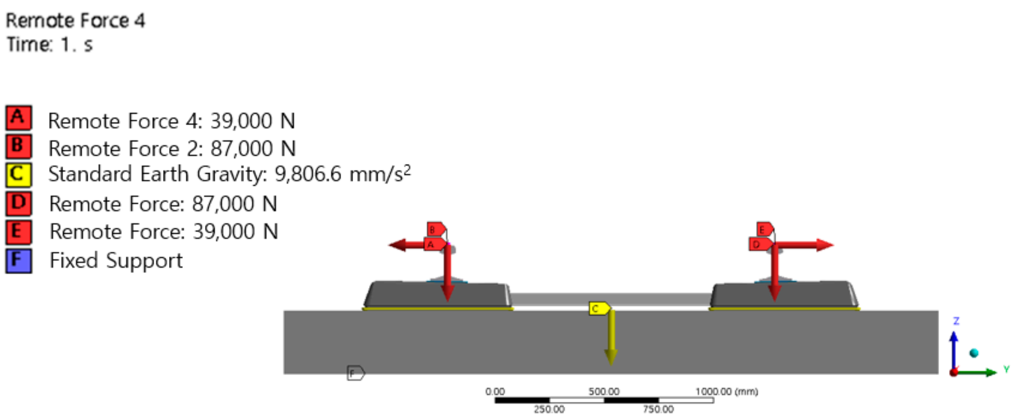

(a)

Figure 5. *Cont.*

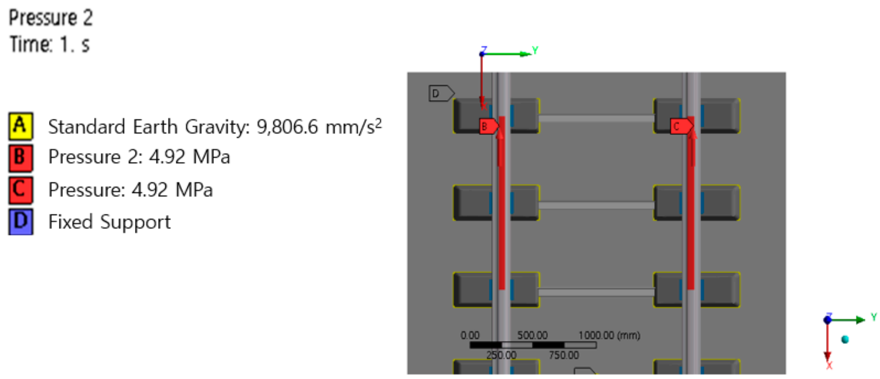

(**b**)

Figure 5. Loading and boundary conditions: (**a**) case 1 train load condition; (**b**) case 2 rail longitudinal pressure condition.

Table 2. Load conditions.

Load Condition			
Case 1		**Case 2**	
Load Case	**Value**	**Load Case**	**Value**
Load case A	Self-weight (Auto cal.)	Load case A	Self-weight (Auto cal.)
Load case B	Measured wheel load (87 kN)	Load case B	Assumed rail pressure (4.92 MPa)
Load case C	Measured lateral wheel load (39 kN)	Load case combination	Load case (A + B)
Load case combination	Load case (A + B + C)		

Figure 5a shows the train load condition of case 1, including the average values of the dynamic wheel load and the lateral force obtained through field measurements, which were 87 kN and 39 kN, respectively.

Figure 5b shows the longitudinal pressure of the rail, which is the same as the braking load of case 2, in the traveling direction of the train. The magnitude of the longitudinal pressure applied to the rail was found by analyzing the equivalent stress of the rubber boot under case 1 condition, and about 4.92–5.2 MPa, which was the longitudinal pressure that generated a similar level of equivalent stress, was applied to the upper surface of the rail head.

To compare and analyze the deformation of the rubber boot according to its material change, the material characteristics of the existing SBR (styrene butadiene rubber) and EP were used as variables in the analysis.

2.4. Numerical Analysis Result

(1) Analysis of Rubber Boot Damage Mechanism and Cause of Damage

To analyze the main damage caused by the position of the rubber boots, the behavior of the RC blocks of the urban railway sleeper floating track was analyzed by applying the load condition as a variable in numerical analysis. For the behavioral characteristics of the RC blocks, the load conditions of case 1 and case 2 were applied, and the results are shown in Figure 6.

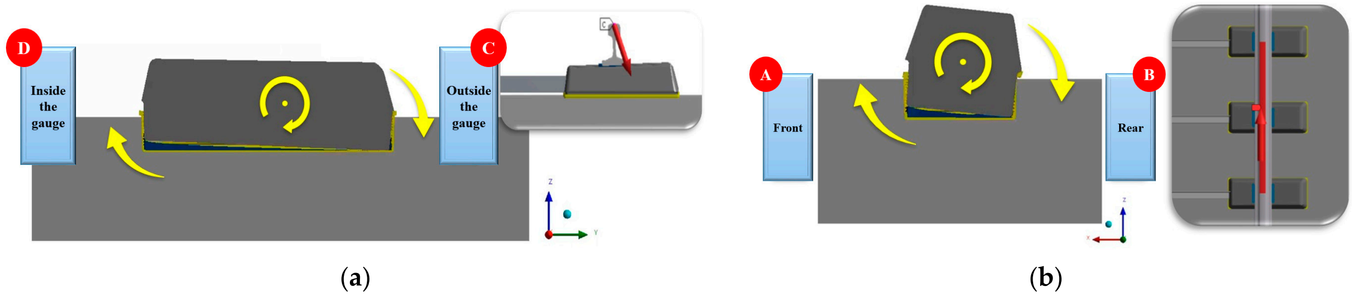

Figure 6. Behavior characteristics of RC blocks: (**a**) case 1; (**b**) case 2.

The structure of the RC sleeper of STEDEF involved fixing the inside of the gauge with a tie bar and leaving the outside of the gauge free. The direction of the resultant force of the load acted outside the gauge because of the dynamic wheel load and dynamic lateral pressure of the train load. Due to the rotational behavior of the sleeper caused by the train load in case 1, as shown in Figure 6a, the side of the rubber boot, outside the gauge, was pressed from the top to bottom. For the rail longitudinal pressure condition of case 2, the sleeper rotated in the direction shown in Figure 6b because of the direction of the applied load and the soft resilient pad directly beneath the RC block.

As shown in Figure 7a, the equivalent stress was concentrated in the side surfaces C and D of the rubber boot made of the existing SBR material, and excessive deformation and strain deviation were relatively large. Moreover, the fluctuation width of the equivalent stress occurred at the edge of the floor boundary. The location derived from numerical analysis and the actual damaged area of the rubber boot (analyzed from the visual inspection of the field sample) coincided. Thus, the main cause of damage to cross-sections C and D was excessive deformation due to the train load.

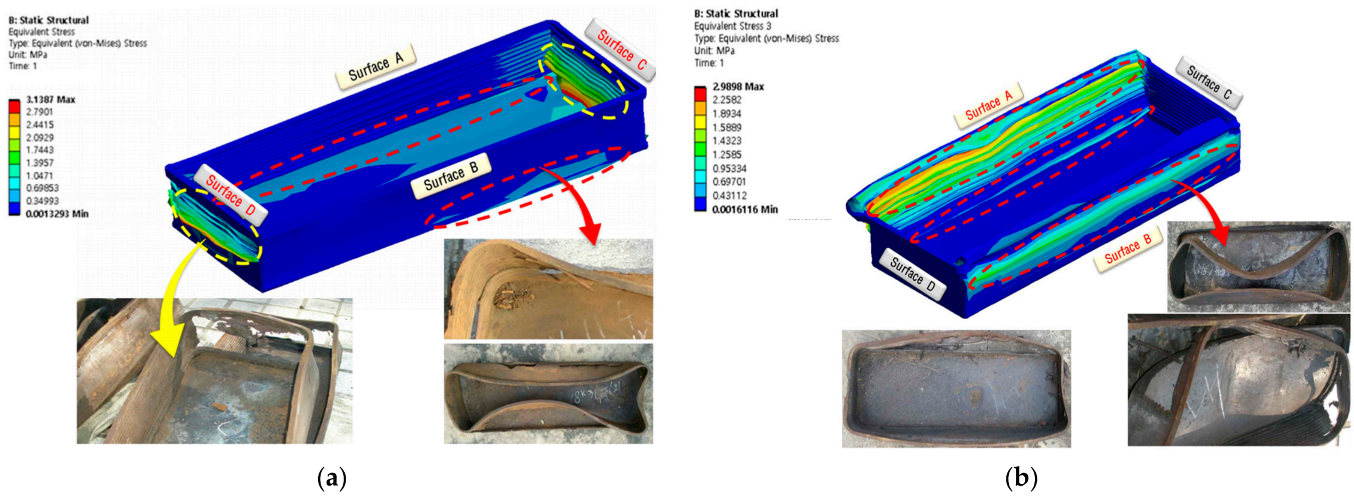

Figure 7. Behavioral characteristics of RC blocks: (**a**) case 1; (**b**) case 2.

In case 2, where the braking load (the largest train load among the longitudinal loads borne by the track) was considered, the equivalent stress was concentrated in cross-sections A and B, which are the front and rear parts, respectively. The deviation of the strain occurred in the existing SBR rubber boot, as shown in Figure 7b. The fluctuation width of the equivalent stress occurred at the edge of the floor boundary. The location derived from the numerical analysis and the actual damaged area of the rubber boot (analyzed through a visual inspection of the field sample) coincided.

(2) Analysis of Rubber Boot Deformation According to Material Change

To analyze rubber boot deformation according to material change, a comparative analysis was performed. The analysis was based on the strain generated by the rubber boot material according to the load condition when the height of the rubber boot was 100 mm. For deformation review, the rubber boot cross-section was set to cross-section C—the side part of the rubber boot that was vulnerable to damage by the train load, as shown in Figure 6b. The results of the deformation analysis for each material are shown in Figure 8.

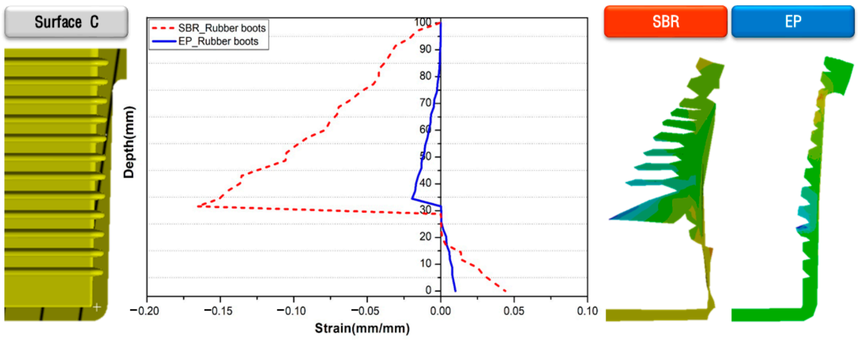

Figure 8. Deformation of rubber boots according to material change.

Based on our analysis of the deformation characteristics of the rubber boots, as shown in Figure 8, a strain of about −0.0009 to 0.044 mm/mm occurred at cross-section C for the existing SBR boots. In particular, the location where the maximum strain occurred was about 30 mm from the lower surface, and the deviation of the strain was very large. On the other hand, for the EP material, a strain of about −0.02 to 0.01 mm/mm occurred at the side cross-section C, but as shown in Figure 8, the size and deviation of the overall strain were smaller than those of the existing SBR material. In the existing SBR material, approximately 90% or more were reduced at the location where the maximum strain occurred.

Figure 9 shows the relationship between displacement and strain generated by the position of the rubber boots.

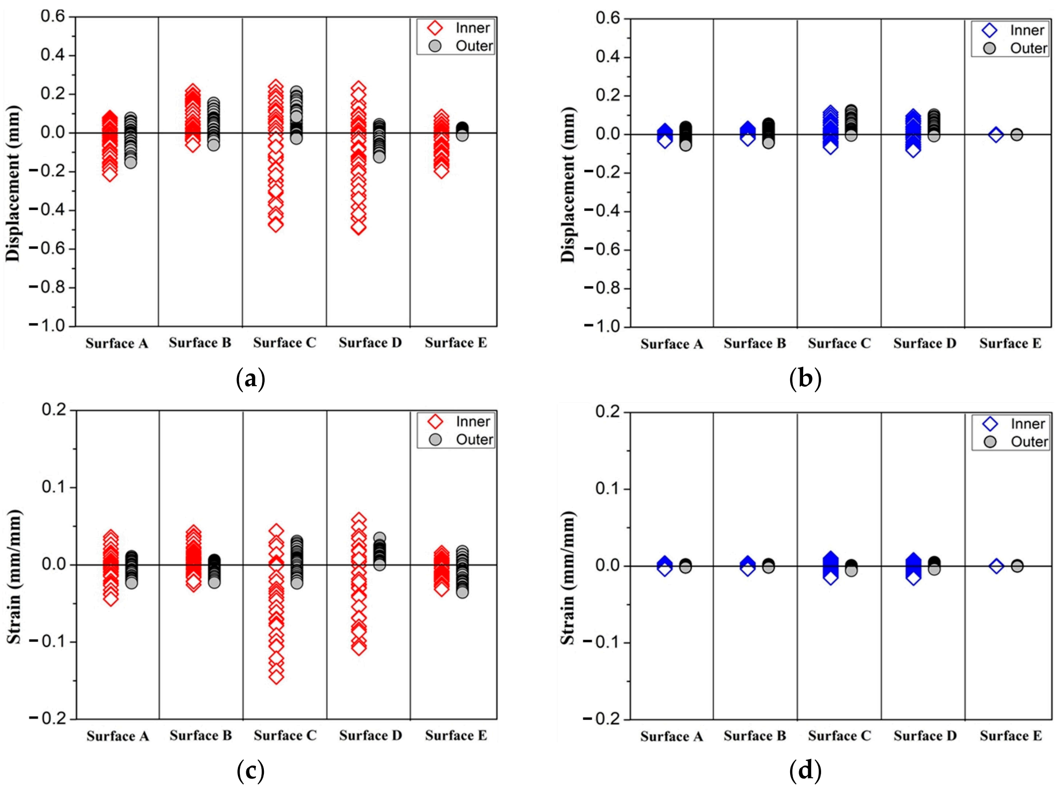

Figure 9. Displacement and strain by the position of the rubber boots: (**a**) SBR displacement; (**b**) displacement; (**c**) SBR strain; (**d**) EP strain.

The displacement and analysis results according to the location of each material of the rubber boot are shown in Figure 9.

In Figure 9a,c, the SBR boots show a large deviation in displacement and strain compared with the EP rubber boots seen in Figure 9b,d. In particular, the size of the displacement and strain generated at cross sections C and D were reduced by about 83% and 90%, respectively, compared with SBR materials.

(3) Equivalent stress analysis of rubber boots according to material change

In this study, to analyze the deformation of the rubber boots according to changes in the material and to investigate the possible extent of damage reduction, the equivalent stress of the rubber boots for each material was calculated according to the load condition, and the results are shown in Figures 10 and 11.

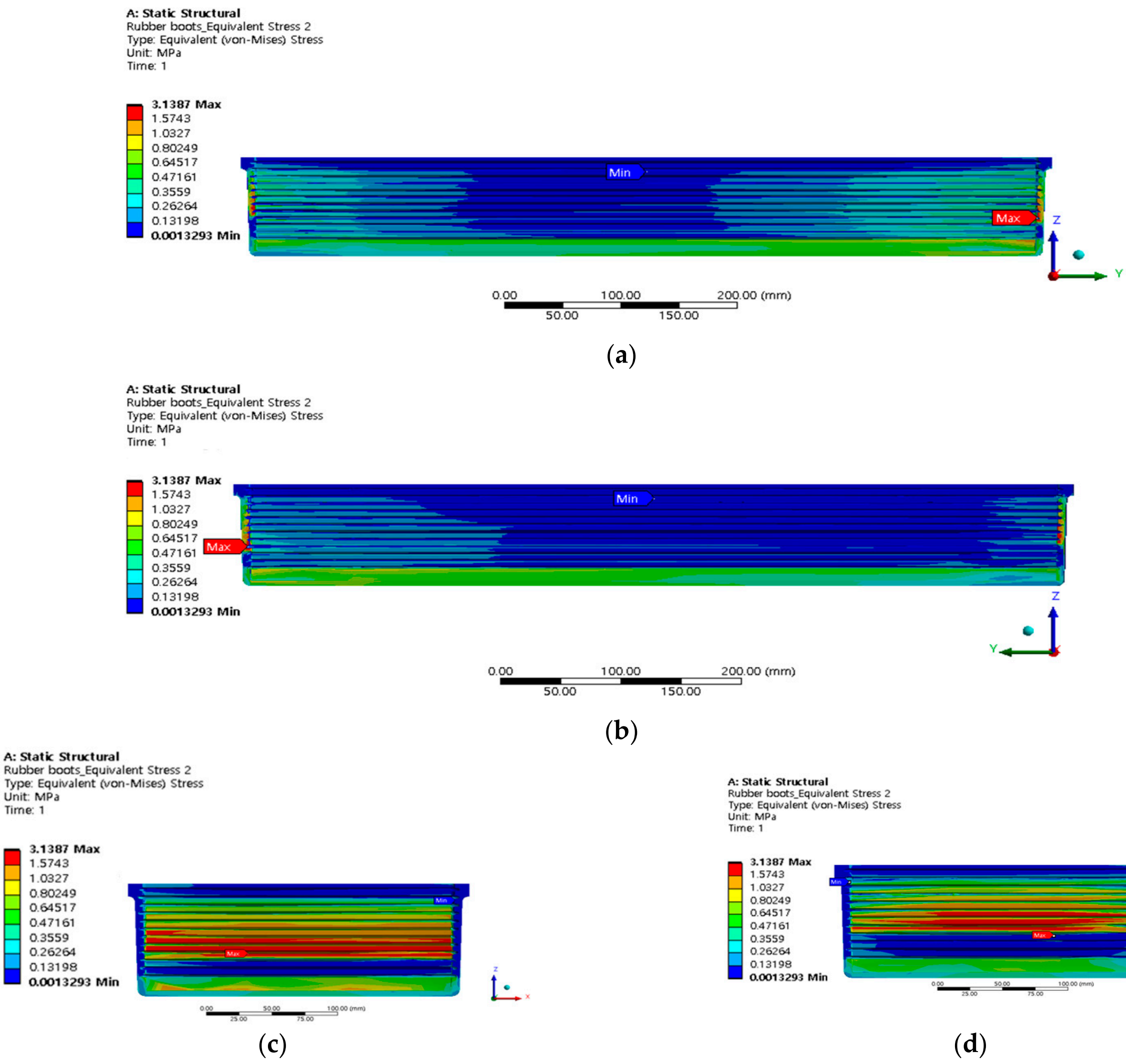

Figure 10. *Cont.*

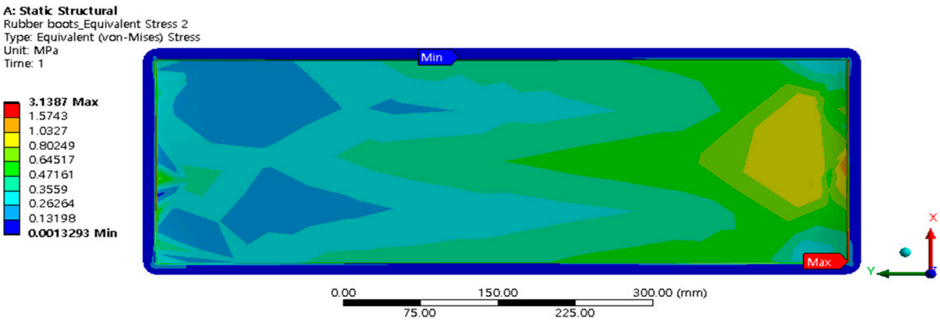

(**e**)

Figure 10. Equivalent stress of the rubber boots made of SBR: (**a**) front part A; (**b**) rear part B; (**c**) side part C; (**d**) side part D; (**e**) floor surface E.

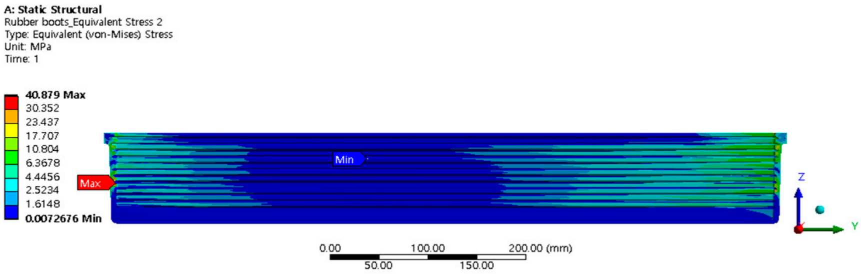

(**a**)

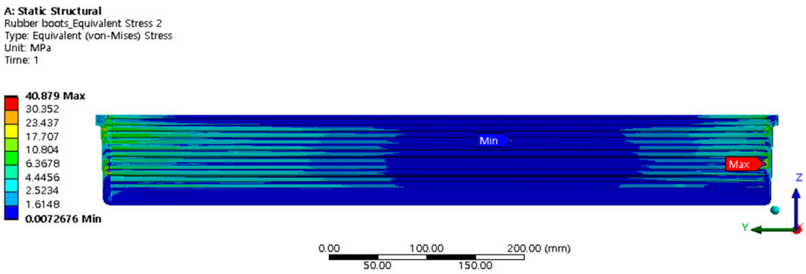

(**b**)

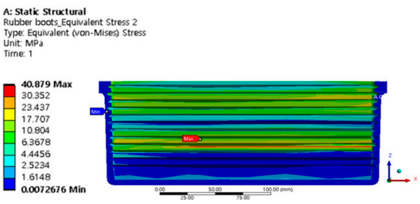

(**c**)

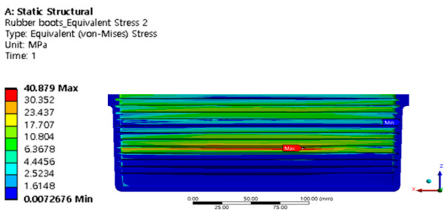

(**d**)

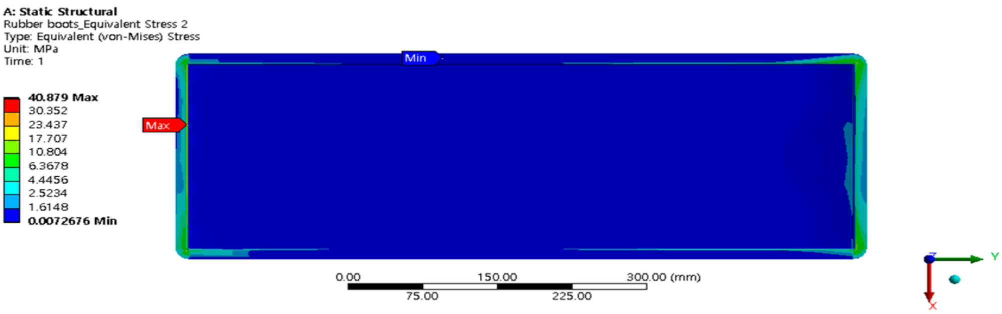

(**e**)

Figure 11. Equivalent stress of the rubber boots made of EP: (**a**) front part A; (**b**) rear part B; (**c**) side part C; (**d**) side part D; (**e**) floor surface E.

The analysis of the equivalent stress of the SBR boots, as shown in Figure 10e, revealed that the equivalent stress was concentrated at the edge of the floor boundary that was in direct contact with the concrete bed. Also, Figure 10c,d confirm that the equivalent stress is concentrated on the internal bumps of cross-sections C and D due to the behavior of the RC block in Figure 5a.

For the EP rubber boot, the equivalent stress was found to be concentrated in the internal bumps on the side surfaces, as shown in Figure 11c,d. Nonetheless, as the distribution of equivalent stress, generated from the internal, was relatively evenly distributed compared with that of the existing SBR material, the phenomenon of equivalent stress concentration was eliminated in the bumps and bottom boundary, and therefore the equivalent stress was also evenly distributed in the floor boundary and surface.

In Figure 11a,c, the EP boots show a small deviation in displacement and strain compared with the SBR rubber boots shown in Figure 11b,d. In particular, the size of the displacement and strain generated at cross-sections A and B were reduced by approximately 90% and 94%, respectively, compared with SBR materials.

(4) Deformation Analysis of Rubber Boots According to Shape Change

In this study, shape design and prototype formation were carried out to derive the optimal shape of the rubber boot. A total of four types of rubber boots were designed to determine the optimal shape (draft). Figure 12 shows the proposed shapes of the rubber boot.

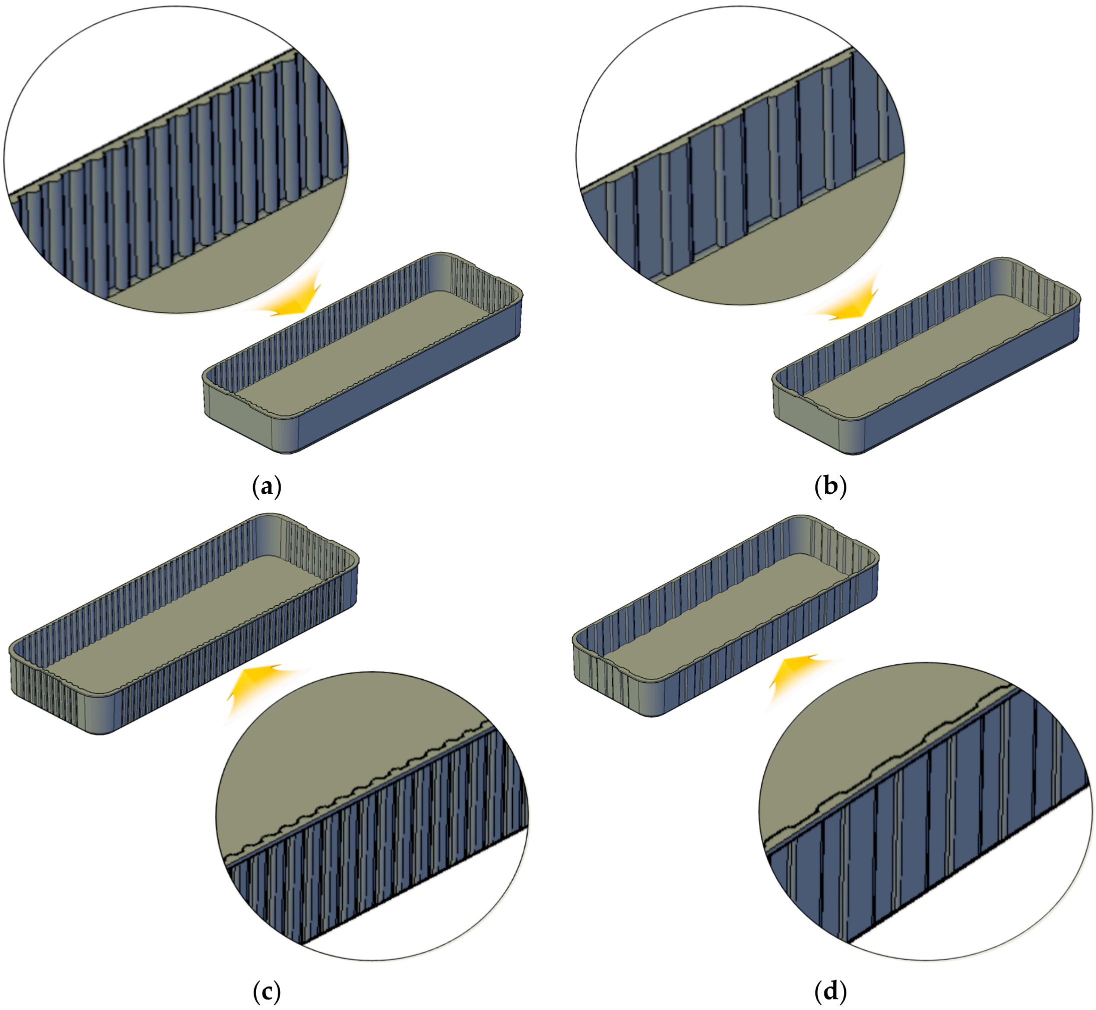

Figure 12. Rubber boot shape design (draft): (**a**) type 1; (**b**) type 2; (**c**) type 3; (**d**) type 4.

In this study, after designing all the possible rubber boot shapes (draft), the products were manufactured in a small size using a 3D printer, as shown in Figure 13.

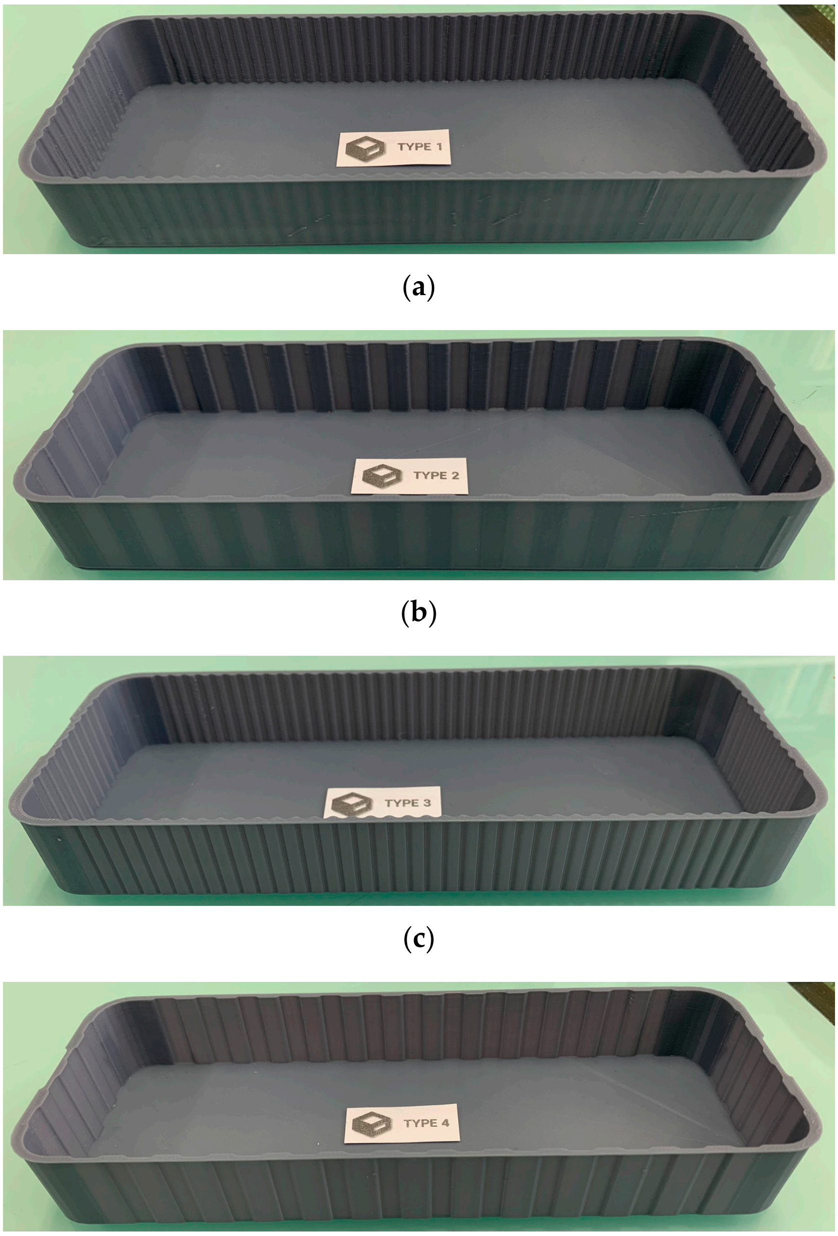

(d)

Figure 13. Rubber boot 3D-printed models (draft). (**a**) type 1; (**b**) type 2; (**c**) type 3; (**d**) type 4.

Numerical analysis was used to analytically confirm the improvement in using the proposed shapes and materials. The entire modeling was performed for the analysis, as shown in Figure 14a [14]. The rubber boots were modeled as a 3D solid element for each shape, as shown in Figure 14b–e [14]. The mechanical properties of the rubber boot obtained from Tables 1 and 2 were applied. For the boundary conditions, all the lower surfaces of the analysis model were fixed. As for the load conditions used in the numerical analysis, as shown in Table 2, a wheel load of 87 kN and a lateral wheel load of 39 kN were applied.

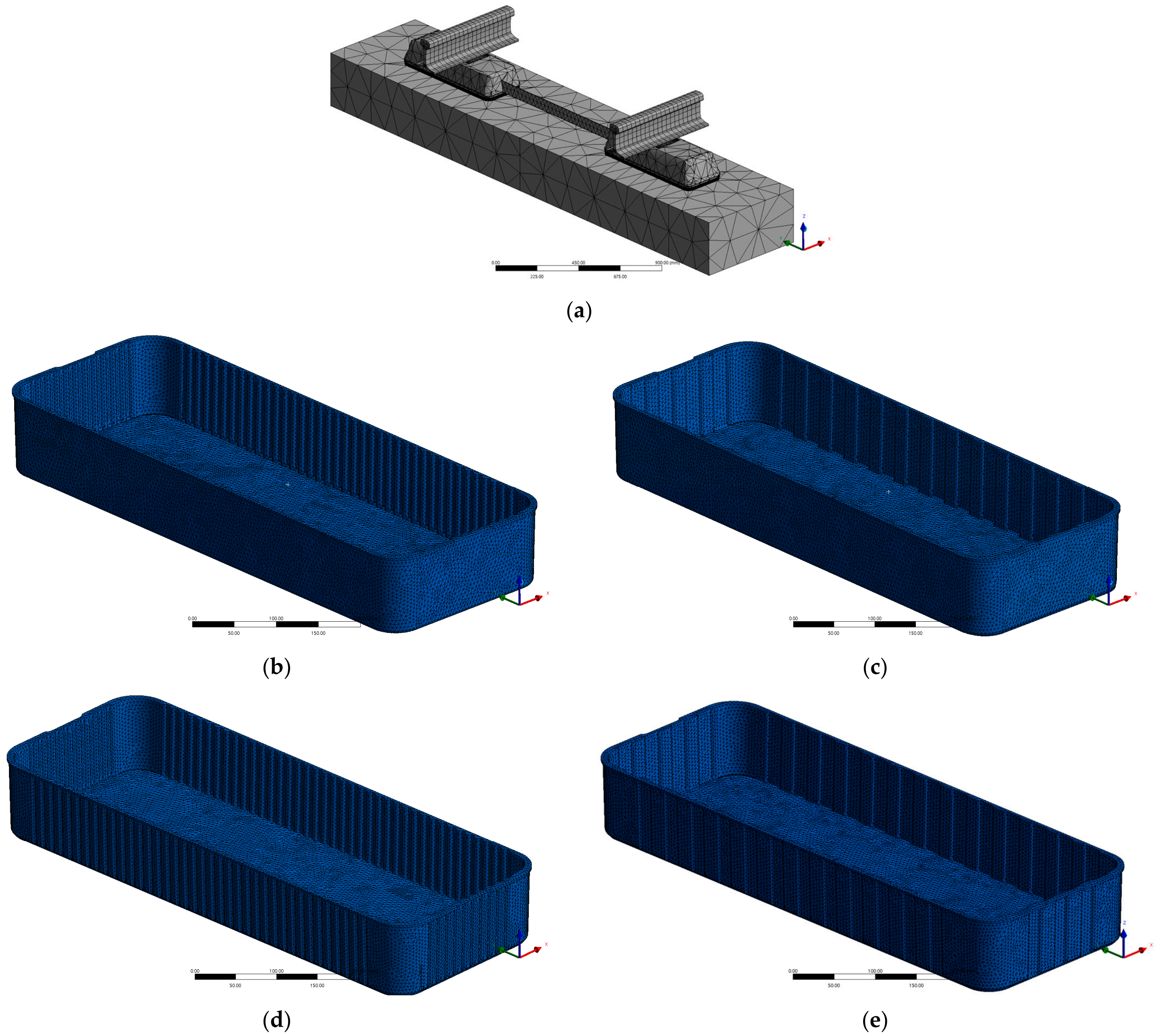

Figure 14. Numerical analysis full modeling: (**a**) full mesh modeling; (**b**) type 1; (**c**) type 2; (**d**) type 3; (**e**) type 4.

The results of the numerical analysis revealed differences in all the positions where the stress of 5 MPa or more occurred, as shown in Figure 15a–d. Stress was observed to be concentrated in the lower surface by the lower bumps for all four shapes. Additionally, stress was concentrated in the corner part. However, the stress level was minutely compared to the stress at which failure could occur. In types 1, 2, and 4, the stress outside the rubber boot was negligible. In type 3, the stress generated inside was transferred to the outside, and the stress was concentrated.

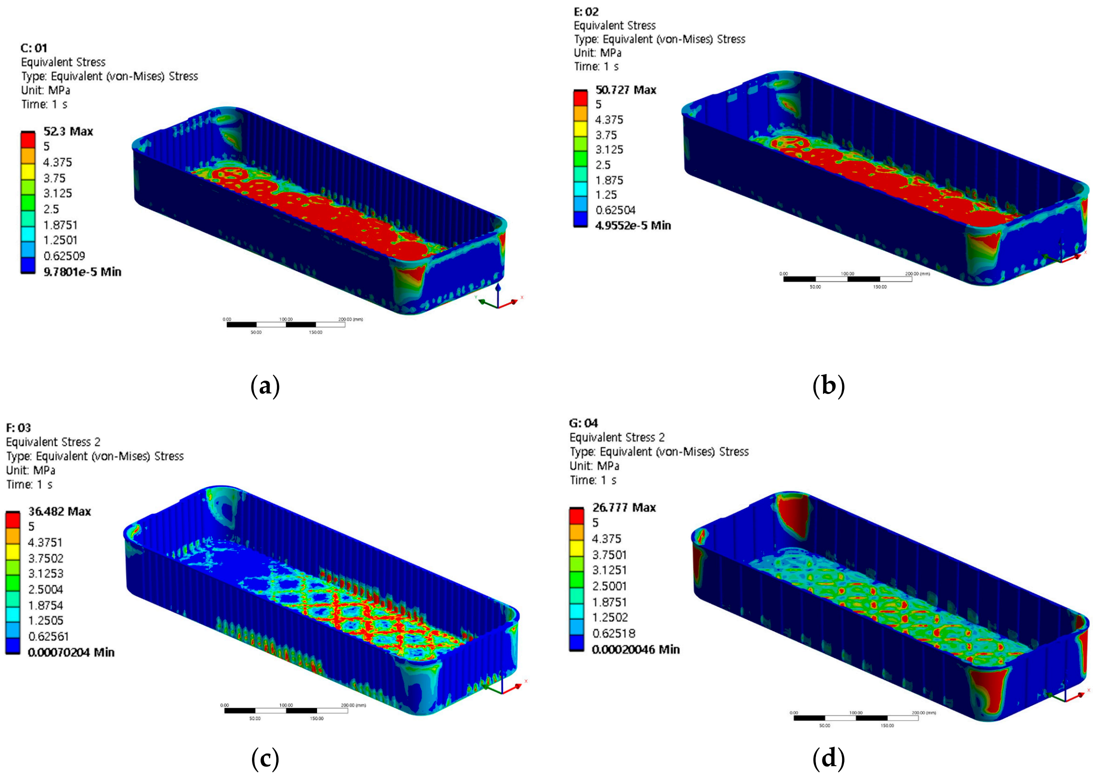

Figure 15. Numerical analysis results for each type of rubber boots: (**a**) type 1; (**b**) type 2; (**c**) type 3; (**d**) type 4.

As a result of numerically analyzing the existing shape of the rubber boot, a position was identified where shear occurred in the horizontal direction because of the direction of the internal bumps, as shown in Figure 16. As a result, the proposed boot shape was designed with the direction of bumps opposite to the previous one, and the currently observed shear deformation did not occur.

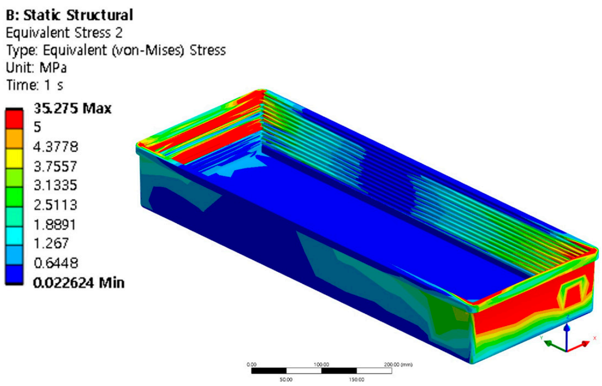

Figure 16. Numerical analysis of existing rubber boot.

3. Indoor Test

3.1. Indoor Test for Optimal Material Selection for Rubber Boots (Material Test Piece)

To select the optimal material for the new eco-friendly rubber boot, the physical properties of various EP materials, as shown in Table 3, were examined, and the priority of the optimal material was determined based on the indoor test. Correspondingly, a total of five seat-type prototypes for indoor testing were produced. Figure 17a–d show the indoor test specimens.

Table 3. PA6 (POLYAMIDE major-grade property comparison table).

Property	ASTM	Unit	PA6	PA6 + ST	PA6 +GF15%	PA6 +GF20%	PA6 +GF30%	PA6 +MF30%
Specific gravity	D 792	-	1.14	1.06	1.24	1.27	1.36	1.31
Hardness	D 785	R-Scale	120	105	120	121	122	110
Tensile strength	D 638	kg/cm^2	750	500	1300	1400	1750	500
Elongation	D 638	%	50	180	5	3.5	3.0	10
Flexural strength	D 790	kg/cm^2	1050	450	1700	1900	2300	700
Flexural modulus	D 790	kg/cm^2	25,000	140	48,000	53,000	79,000	30,000
Impact strength	D 256	kg.cm/cm	4.5	60.0	6.0	8.0	9.0	8.0
Melting point	D S C	°C	220	220	220	220	220	220
Heat-deflection temperature	D 648	°C	175	120	205	220	220	150
Flame resistance	18.6 kg/cm^2	50	190	205	210	60		
Mold shrinkage rate	UL 94	-	HB	HB	HB	HB	HB	HB
Quality	D 955	%	1.4	1.8	0.7	0.6	0.5	0.3

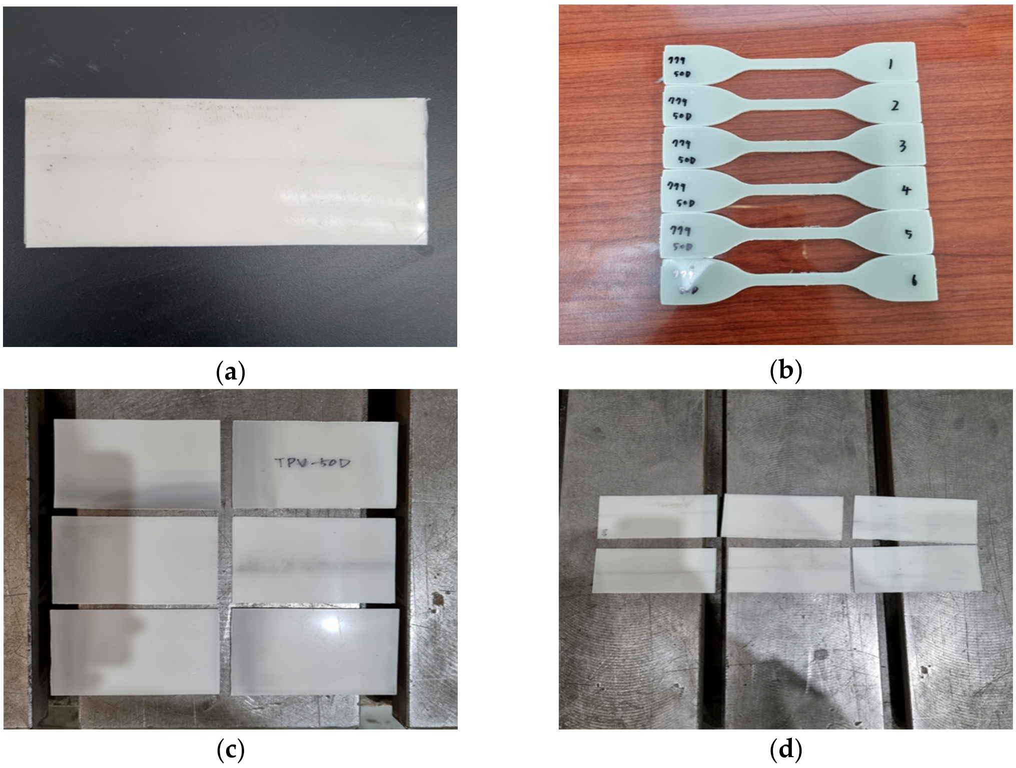

Figure 17. Rubber boot indoor test specimen (example): (**a**) hardness; (**b**) tensile strength; (**c**) shear; (**d**) static/dynamic compression.

For the indoor tests, hardness, tensile strength, shear, static compression, and dynamic compression tests were performed, as shown in Figure 18a–d. Figure 18 shows the photographs of the indoor tests.

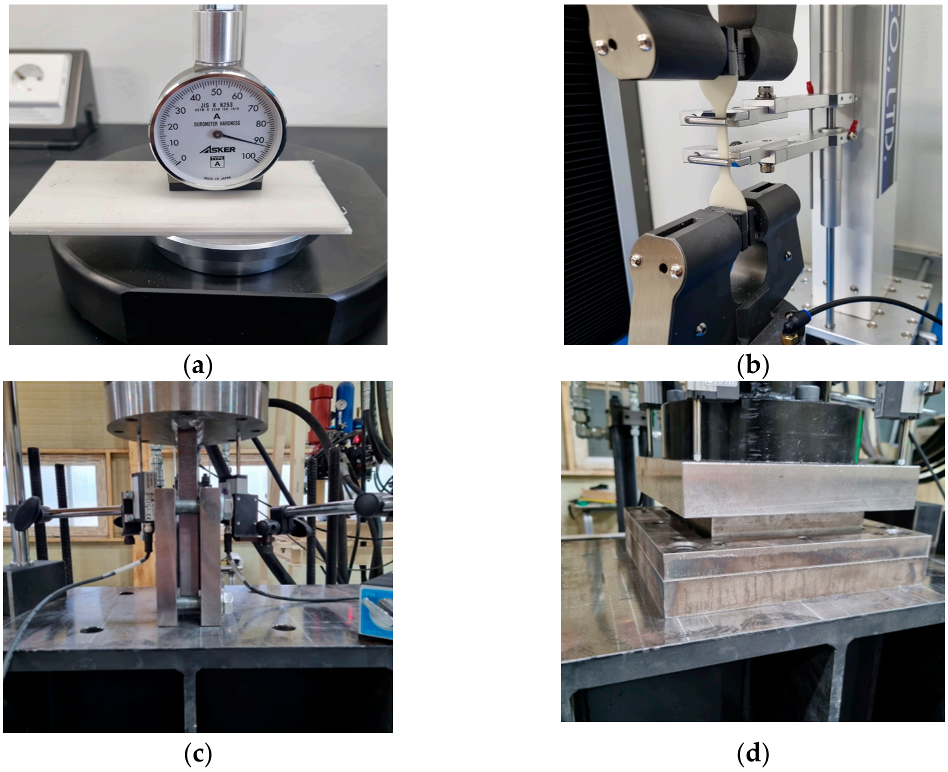

Figure 18. Indoor material test view: (**a**) hardness test; (**b**) tensile strength test; (**c**) shear test; (**d**) static/dynamic compression test.

As the indoor tests must satisfy the performance requirements listed in Table 4, it was tested whether hardness, static compression, dynamic compression, and shear tests satisfied KRSA-T-2017-1001-R0 and whether tensile strength satisfied ASTM D638. These indoor tests were selected because they are essential when reviewing the performance of rubber boots in South Korea.

Table 4. Performance requirements.

Test Item	Unit	Performance Requirements (Performance Criteria)		Target	Experiment Result	Test Code
1. Hardness	Shore A	58~68		68	98	KRSA-T-2017-1001-R0
2. Tensile strength	kg/cm^2	Before aging 150	After aging 120	150 or more before and after aging	1783 before and after aging	ASTM D638
3. Static shear strength	kg/mm	200 or less		200 or more	10,706	KRSA-T-2017-1001-R0
4. Static compressive strength	kg/mm	1200~2300		2300 or more	28,915	KRSA-T-2017-1001-R0
5. Dynamic Compressive Strength	kg/mm	2000~4200		4200 or more	79,251	KRSA-T-2017-1001-R0

The hardness test was performed according to KS M 6519, as shown in Figure 8a.

To identify the EP material properties of a rubber boot, tensile tests were conducted for EP members according to ASTM D638. Each specimen was installed and loaded using a universal testing machine with 500 kN capacity, as shown in Figure 8b. The specimens were loaded up to failure with a speed of 5 mm/min according to the displacement control method. Hardness, static compression, dynamic compression, and static shear strength were tested according to KRSA-T-2017-1001-R0 and KS M 6518 [16].

The results of the static shear strength test are shown in Figure 8c, for which a compressive load of 8 kN was applied at a speed of 24 ± 4.8 kN/min. Additionally, the load was increased up to 1.5 kN at the side part for a compression rate of 3 ± 0.6 kN/min.

For the static compressive strength test, a load of 1 kN was applied to the steel plate at a speed of 3 ± 0.6 kN/min. After 1 min, the sensor was set to 0, and a load of 21 kN was loaded at a load speed of 24 ± 4.8 kN/min. In the dynamic compressive test, the extent of displacement was measured by applying a load of 1 kN to 22 kN for 1 min at a 5 Hz cycle. The results of static and dynamic compressive tests are shown in Figure 8d.

Based on the indoor test analysis, as shown in Figure 19, all materials exceeded the target value for tensile strength before the aging test. After the aging test, all materials except 50D exceeded the target value of tensile strength.

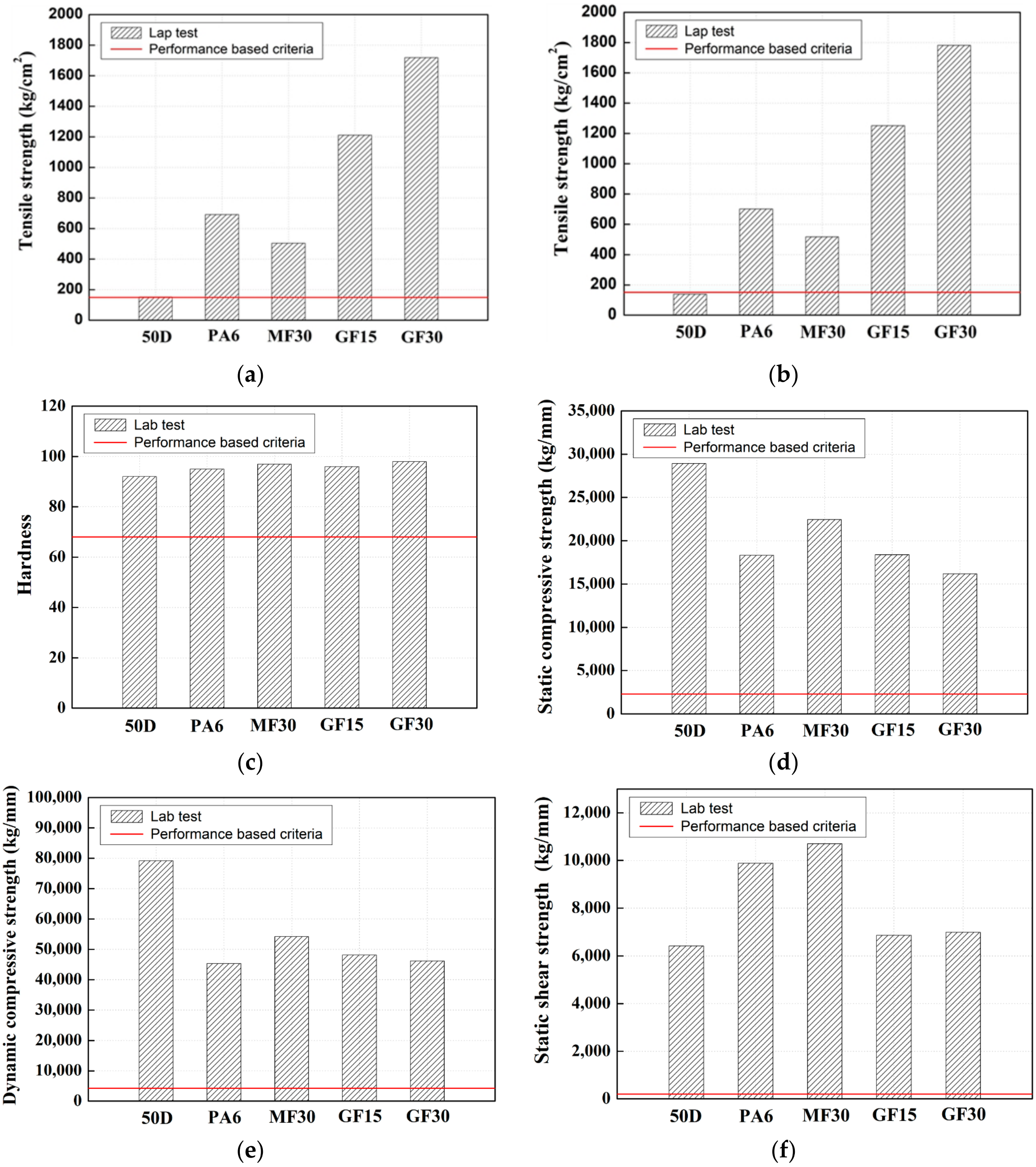

Figure 19. Indoor test analysis results: (**a**) tensile strength before the aging test; (**b**) tensile strength after the aging test; (**c**) hardness; (**d**) static compressive strength; (**e**) dynamic compressive strength; (**f**) static shear strength.

Furthermore, all materials exceeded the target values for hardness, static compressive strength, dynamic compressive strength, and static shear strength. Most of the EP materials reviewed in this study sufficiently met the corresponding criteria; thus, the optimal material was derived in consideration of future manufacturability and economic feasibility.

3.2. Indoor Test for Selecting the Optimal Shape of the Rubber Boot (Actual Test Piece)

The physical specimens using the four shapes were fabricated and tested to investigate the effect of improving the rubber boot shape. The specimens in the physical test are shown in Figure 20. The actual test was performed for static compressive strength and shear strength, as shown in Figure 21.

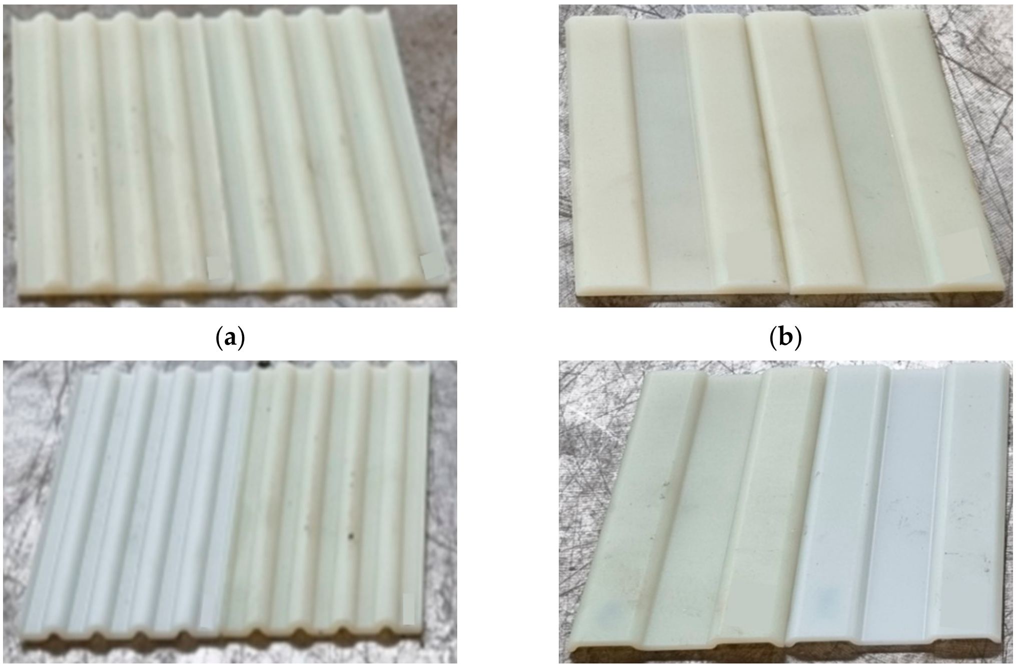

(a) (b) (c) (d)

Figure 20. Physical test specimen: (**a**) type 1; (**b**) type 2; (**c**) type 3; (**d**) type 4.

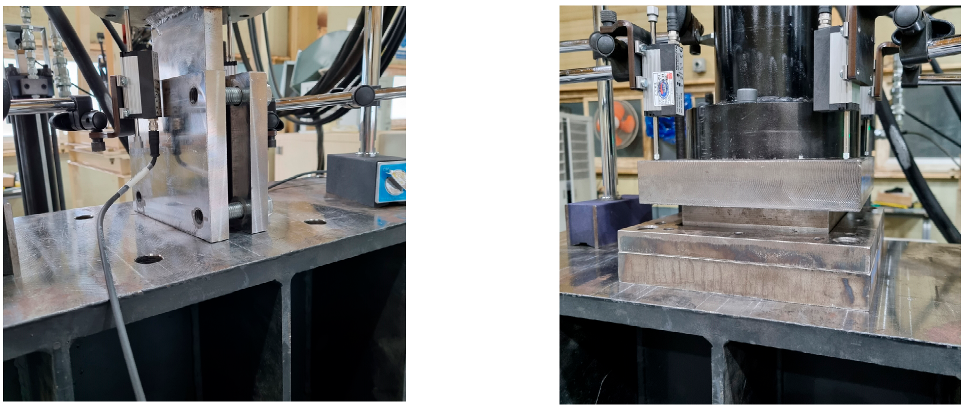

(a) (b)

Figure 21. Indoor test view: (**a**) static compressive strength; (**b**) static shear strength.

As shown in Figure 22a, the actual indoor test results verified that the compressive strength was over the target performance of 2300 kg/mm (compared with the performance requirements of 1200–2300 kg/mm). In terms of the static compressive strength, a performance improvement of approximately 1.29–7.82 times from type 1 to type 4 was confirmed.

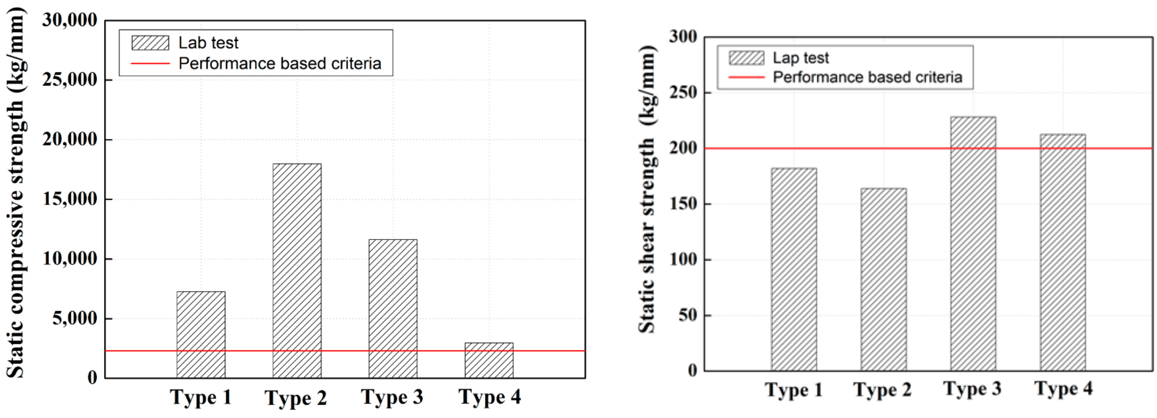

(**a**) (**b**)

Figure 22. Indoor test analysis results (**a**) static compressive strength; (**b**) static shear strength.

As shown in Figure 22b, type 3 and type 4 satisfied the performance requirements for the static shear strength test. Type 3 showed 28 times the shear performance effect, and type 4 showed 6 times the shear performance effect. Therefore, the type 3 rubber boot was proven to satisfy the most target performance in this study.

4. Conclusions

In this study, the cause of damage and vulnerable sections of rubber boots, one of the track components of urban railway STEDEF, were examined through visual inspection and numerical analysis and based on the results, an improvement plan was proposed.

Through the visual inspection of the field samples, the main causes of damage to the rubber boots occurred due to two main reasons: lack of material stiffness and internal bumps of the rubber boots. Through the visual inspection and numerical analysis of field samples, it was discovered that the rubber boots in contact with the RC blocks were subjected to excessive deformation due to the concentration of equivalent stress and displacement at the edge of the side and bottom boundaries, which made these boundaries vulnerable to damage.

Through numerical analysis, we observed that the behavior of the RC blocks on the STEDEF track (according to the load conditions) caused damage to the side of the rubber boots through internal and external rotation of the gauge. Likewise, when the longitudinal pressure of the rail, such as a braking load, rotated in the front and rear directions of the rubber boots, it caused damage to these areas.

The material of the existing rubber boots currently in use is SBR, which is a synthetic rubber material, and the shape of existing SBR rubber boots is deformed due to long-term train load. In addition, the stiffness of this material is insufficient, and wear resistance performance, stress, and displacement occur owing to deformation and friction with the RC sleeper. Numerical analysis and experiments were performed by applying EP to a rubber boot as a substitute for SBR. As a result, for the proposed EP rubber boot, the magnitude of displacement and strain generated by position was reduced by about 83% to 90% compared with the existing SBR boots.

Through visual inspection and numerical analysis, we found that the damage was caused by excessive deformation, as the lack of material stiffness of the rubber boots and the rotation of the RC blocks resulted in deformation concentration in the microsections. Furthermore, the damage location of the aging rubber boots coincided with the location where equivalent stress was concentrated, and excessive deformation occurred based on the numerical analysis.

In conclusion, EP material effectively reduces damage, as it has sufficient material strength and thus greatly reduces the generated stress and deformation in rubber boots. Lastly, as the shape of the internal bumps in rubber boots competes with sleepers in stress behavior, which results in concentrated stress in the irregular parts, if the type 3 shape is used, excessive displacement and stress generation in the rubber boots can be prevented. In the future, we plan to research the application of the improved rubber boot proposed.

Author Contributions: Conceptualization, J.-Y.C., H.S.P. and J.-S.C.; methodology, J.-Y.C.; software, J.-Y.C., H.S.P. and S.-H.K.; formal analysis, H.S.P. and S.-H.K.; resources, H.S.P.; data curation, J.-Y.C., H.S.P. and J.-S.C.; writing—original draft preparation, J.-Y.C. and S.-H.K.; writing—review and editing, S.-H.K. All authors have read and agreed to the published version of the manuscript.

Funding: This research received no external funding.

Institutional Review Board Statement: Not applicable.

Informed Consent Statement: Not applicable.

Data Availability Statement: Not applicable.

Conflicts of Interest: The authors declare no conflict of interest.

References

1. Choi, J.Y.; Bong, J.G.; Han, J.M.; Chung, J.S. Dynamic behavior of sleeper floating track system (STEDEF) on urban rapid transit according to replacement of resilience pad. *J. Converg. Cult. Technol.* **2020**, *6*, 335–340.
2. Lee, D.W.; Park, Y.G.; Choi, J.Y. A study on the evaluation of track support stiffness on the various track type in urban transit. *J. Korean Soc. Railw.* **2011**, *14*, 262–270. [CrossRef]
3. Kim, H.S. Damage Effect Analysis for Track Components of Sleeper Floating Track in Urban Transit. Ph.D. Thesis, Dongyang University, Yeongju-si, Republic of Korea, February 2021.
4. Kim, H.S. An Influence of the Fastening Force on the Rail Force of the Curved Track in Urban Railway. Master's Thesis, Seoul National University of Science and Technology, Seoul, Republic of Korea, February 2016.
5. Lee, S.S. A Study on the Performance of the Track Reduction Material of Vibration on the Scene of Busan Urban Railway No. 2 Line. Master's Thesis, Woosong University, Daejeon, Republic of Korea, February 2013.
6. Vu, L.; Jang, D.D.; Kang, Y.S. Assessment of structural dynamic response and vehicle-track interaction of precast slab track systems. *Appl. Sci.* **2021**, *11*, 3558. [CrossRef]
7. Vu, L.; Kang, Y.S. Land transfer efficiency based on structural deflection assessment of the precast floating track. *Appl. Sci.* **2021**, *11*, 120. [CrossRef]
8. Li, D.; Zhang, Y.; Miao, Q.; Cui, R. Experimental study on the vibration control effect of long elastic sleeper track in subways. *Shock Vib.* **2018**, *2018*, 6209518.
9. Ferdous, W.; Manalo, A.; Erp, G.V.; Aravinthan, T. Evaluation of an innovative composite railway sleeper for a narrow-gauge track under static load. *J. Compos. Constr.* **2018**, *22*, 07018001. [CrossRef]
10. Ferdous, W.; Manalo, A.; Erp, G.V.; Aravinthan, T.; Kaewunruen, S.; Remennikov, A. Composite railway sleepers-recent developments, challenges and future prospects. *Compos. Struct.* **2015**, *135*, 158–168. [CrossRef]
11. Ju, S.; Yoon, J.; Sung, D.; Pyo, S. Mechanical properties of coal ash particle-reinforced recycled plastic-based composites for sustainable railway sleepers. *Polymers* **2020**, *12*, 2287. [CrossRef] [PubMed]
12. Smirnov, V. Dynamic analysis of railway track with vibration isolated booted sleepers. In Proceedings of the MATEC Web of Conferences 196, Rostov-on-Don, Russia, 3 September 2018; Volume 01045.
13. Gupta, S.; Liu, W.F.; Degrande, G.; Lombaert, G.; Liu, W.N. Prediction of vibrations induced by underground railway traffic in Beijing. *J. Sound Vib.* **2008**, *310*, 608–630. [CrossRef]
14. Kim, S.H. Damage Cause Analysis of Rubber Boots for Sleeper Floating Track System in Urban Transit. Master's Thesis, Dongyang University, Yeongju-si, Republic of Korea, February 2022.
15. ANSYS Inc. *ANSYS Workbench 2021 R1*; ANSYS Inc.: Cannonsberg, PA, USA, 2021.
16. *KS M 6519*; Method of Analysis for Rubber Goods. Korean Agency for Technology and Standards: Eumseong, Republic of Korea, 2018.